Journal of Sound and Vibration 481 (2020) 115448

Contents lists available at ScienceDirect

Journal of Sound and Vibration

journal homepage: www.elsevier.com/locate/jsvi

A novel damage index for damage detection and localization of plate-type structures using twist derivatives of laser-measured mode shapes

Wei Xu [a, b], Weidong Zhu [a, *], Maosen Cao [b], Hao Wu [c, b], Ruihu Zhu [d]

[a] Department of Mechanical Engineering, University of Maryland, Baltimore County, Baltimore, MD, 21250, United States
[b] Department of Engineering Mechanics, Hohai University, Nanjing, 210098, China
[c] China Energy Engineering Group Anhui Electric Power Design Institute Co., Ltd, Hefei, 230601, China
[d] College of Harbour, Coastal and Offshore Engineering, Hohai University, Nanjing, 210098, China

ARTICLE INFO

Article history:
Received 15 January 2020
Received in revised form 3 April 2020
Accepted 9 May 2020
Available online 14 May 2020
Handling Editor: K. Shin

Keywords:
Structural damage detection
Plate
Mode shape
Twist derivative
Multi-resolution analysis
Laser scanning measurement

ABSTRACT

It is important to detect and locate local damage in plate-type structures before such damage develops to a significant degree, jeopardizing the integrity and safety of structures. To address this problem, approaches using derivatives of laser-measured mode shapes have become the research focus during the recent decade. In a physical sense, damage can cause discontinuities in shear strains; conversely, such discontinuities can be reflected in twist derivatives of mode shapes, whereby the presence of the damage can be manifested. To address the susceptibility of twist derivatives to noise interference, this study formulates a new concept of multi-resolution twist derivative by integrating the multi-resolution analysis into twist derivatives, which features higher robustness against noise interference. A novel damage index using multi-resolution twist derivatives is established for detecting and locating damage in plate-type structures. In particular, a strategy of choosing mode shapes and a scheme of sparsely sampling them are proposed. By numerical simulation using the finite element method, the capability of the approach is numerically verified on a plate-type structure with a square notch. The applicability of the method is experimentally validated by detecting and locating a notch on an aluminum plate, whose mode shapes are acquired through non-contact measurement using a scanning laser vibrometer. The numerical and experimental results show that the approach can accurately characterize the presence, location, and size of the damage, and is robust against noise interference, suitable for detecting and locating damage of plate-type structures under noisy conditions.

1. Introduction

Plate-type structural components are widely used in mechanical, aerospace, and civil engineering fields. Damage in plate-type structures can occur and accumulate during the life time of the structures. In order to ensure the integrity and safety of plate-type structural components, methods of damage detection have been widely developed in the past two decades [1–5],

* Corresponding author.
E-mail addresses: wxu@hhu.edu.cn (W. Xu), wzhu@umbc.edu (W. Zhu), cmszhy@hhu.edu.cn (M. Cao), wuhao_hhu@163.com (H. Wu), ruihuzhu@hhu.edu.cn (R. Zhu).

https://doi.org/10.1016/j.jsv.2020.115448
0022-460X/

among which approaches relying on out-of-plane mode shapes have been attracting increasing attention because spatial information contained in a mode shape benefits damage localization [6–9].

As per the theory of thin plates, normal and shear strains are proportional to partial derivatives of mode shapes with respect to spatial coordinates [10]. Damage-induced local changes in the bending stiffness can cause discontinuities in strains at damage locations. Conversely, such discontinuities can cause changes in partial derivatives of measured mode shapes, which can be used to detect and locate damage. Superior to conventional sensors, structural mode shapes can be measured through non-contact laser scanning measurement without effects on stiffness and mass. In the recent decade, damage detection approaches relying on laser-measured out-of-plane mode shapes have become a research focus in the field of vibration-based structural damage detection. Representative approaches from the perspective of normal strains are as follows. Qiao et al. [11] evaluated and compared three typical mode-shape-based algorithms for identification of delamination in composite laminated plates. Xu et al. [12–14] formulated concepts of wavelet curvature mode shapes for damage identification of plates. Superior to conventional curvature mode shapes, wavelet curvature mode shapes feature higher sensitivity to damage and robustness against noise interference. Yang et al. [15,16] proposed the novel concept of Fourier spectral curvature mode shape by using the Fourier spectral method over the conventional central difference operator, whose capacity and superiority in detecting damage was well verified in composite plates. Cao et al. [17,18] introduced the principal component analysis into curvature mode shapes to extract damage-induced local features for damage detection of plate-type structures. Xu et al. [19,20] and Chen et al. [21–23] extracted local anomalies in differences between measured and reconstructed curvature mode shapes to identify damage in plate-type structures. In contrast, much less attention was paid to approaches from the perspective of shear strains. Representative approaches are as follows. Xu et al. [24,25] integrated mode shape derivatives related to both normal strains and shear strains, by which a damage index was established using “pseudo-excitation”. The presence, location, and size can be well characterized by the damage index. Cao et al. [26] revealed the physical sense of shear strain singularity caused by delamination in laminates, built on which derivatives of shear strains were proposed for damage detection of plate-type structures. The method was validated on a glass fiber reinforced polymer laminate that beared a heat-caused delamination. Experimental results show that the approach has the distinctive ability to detect slight delamination in composite laminates.

On the other hand, by taking advantage of non-contact laser scanning measurement, measured mode shapes can be densely sampled so that sampling intervals can match dimensions of small damage. However, superfluous sampling points make the laser scanning measurement time-consuming. In addition, noise interference can be amplified in derivatives of densely sampled mode shapes due to the finite difference method. In consequence, actual damage features can be masked by intense noise interference [12]. Therefore, de-noising processing needs to be applied on mode shapes beforehand. It is noteworthy that the recently developed fast laser scanning strategy using a continuously scanning laser Doppler vibrometer is a promising technology to measure densely sampled mode shapes in a short time [21–23].

With these concerns, from the perspective of shear strains, the concept of twist derivative, which is the fourth-order derivative of a mode shape, is developed for damage detection of plate-type structures in this study. In particular, a strategy of choosing mode shapes and a scheme of sparsely sampling them are proposed. The multi-resolution analysis (MRA) is introduced into twist derivatives to eliminate noise components involved in mode shapes, whereby the new concept of multi-resolution twist derivative (MRTD) is formulated with high robustness against noise interference. Finally, a novel damage index is established for damage detection and localization of plate-type structures under noisy conditions.

The rest of the paper is organized as follows. Section 2 gives fundamentals for the concept of twist derivative, and formulates a new concept of MRTD by integrating twist derivatives with the MRA, based on which a novel damage index is established for damage detection and localization of plate-type structures. Section 3 numerically verifies the capability of the proposed approach on a plate-type structure with a notch with reduced thickness in a square area. Section 4 experimentally validates the applicability of the approach by detecting and locating a square notch in an aluminum plate. The damaged plate is excited using a lead-zirconate-titanate (PZT) piezoelectric actuator, and its mode shapes are acquired through non-contact measurement using a scanning laser vibrometer (SLV). Section 5 presents concluding remarks.

2. Damage index for damage detection and localization

The physical sense of twist derivative in detecting damage is introduced in this section. The MRA relying on the discrete wavelet transform (DWT) is integrated into twist derivatives, whereby the MRTD is formulated with higher robustness against noise interference. A novel damage index is established based on the MRTD for damage detection and localization of plate-type structures.

2.1. Twist derivatives

The equation of out-of-plane motion of a thin plate subject to a transverse excitation can be written as [27]

$$D\nabla^4 w(x,y,t) + \rho h \frac{\partial^2 w(x,y,t)}{\partial t^2} + c\frac{\partial w(x,y,t)}{\partial t} = q, \tag{1}$$

where $w(x,y,t)$ is the out-of-plane displacement of the plate at its mid-surface with respect to coordinates x and y and time t, D is the bending stiffness of the plate, ρ is the material density per unit volume, h is the thickness, c is the damping coefficient, q is the transverse excitation, and $\nabla^4 w$ denotes

$$\nabla^4 w = \frac{\partial^4 w}{\partial^4 x} + 2\frac{\partial^4 w}{\partial^2 x \partial^2 y} + \frac{\partial^4 w}{\partial^4 y}. \tag{2}$$

Assume that the steady-state displacement $w(x,y,t)$ is the product of the mode shape $W(x,y)$ and time response $e^{-i\omega t}$ with i being the imaginary unit and ω the corresponding natural frequency:

$$w(x,y,t) = W(x,y)e^{-i\omega t}. \tag{3}$$

For elements in the plate that bear no transverse load, *i.e.*, $q = 0$, Eq. (1) can be rewritten by substituting Eq. (3) into it:

$$D\nabla^4 W - \omega^2 \rho h W - i\omega c W = 0, \tag{4}$$

where

$$\nabla^4 W = \frac{\partial^4 W}{\partial^4 x} + 2\frac{\partial^4 W}{\partial^2 x \partial^2 y} + \frac{\partial^4 W}{\partial^4 y}. \tag{5}$$

The shear strain γ_{xy} is proportional to the twist κ_{xy}:

$$\kappa_{xy} = \frac{\partial^2 W}{\partial x \partial y}, \tag{6a}$$

$$\gamma_{xy} = -2z\kappa_{xy}, \tag{6b}$$

where z is the transverse coordinate whose origin is at the mid-surface of the plate. Partial derivatives of the twist with respect to x and y are termed as *twist derivatives* hereafter in this paper, denoted as T_{xy}:

$$T_{xy} = \frac{\partial^2 \kappa_{xy}}{\partial x \partial y} = \frac{\partial^4 W}{\partial^2 x \partial^2 y}, \tag{7}$$

whose discrete form can be obtained by the finite difference method:

$$\begin{aligned} T_{xy}[x,y] = \frac{1}{h_x^2 h_y^2}\Big(& W[x-h_x, y-h_y] - 2W[x-h_x, y] + W[x-h_x, y+h_y] \\ & -2W[x, y-h_y] + 4W[x,y] - 2W[x, y+h_y] \\ & +W[x+h_x, y-h_y] - 2W[x+h_x, y] + W[x+h_x, y+h_y]\Big), \end{aligned} \tag{8}$$

with h_x and h_y being the measurement intervals in the x- and y-directions, respectively.

As per Eq. (6b), the twist is proportional to the shear strain in a plate; it can reflect discontinuities in shear strains caused by damage-induced local changes in the bending stiffness of the plate. Conversely, by differentiating the twist with respect to x and y, such discontinuities in the twist derivatives can concentrate in the damage region, by which the presence of the damage can be manifested.

2.2. Multi-resolution twist derivatives

By addressing the susceptibility of the finite difference method to noise interference, the MRA is integrated into twist derivatives using the two-dimensional (2D) DWT. The 2D wavelet function $\psi^{\nu}(x,y)$ ($\nu = 1,2,3$) and scale function $\varphi(x,y)$ can be formulated using the one-dimensional (1D) wavelet and scaling functions [28]:

$$\psi^1(x,y)=\varphi(x)\psi(y), \tag{9a}$$

$$\psi^2(x,y)=\psi(x)\varphi(y), \tag{9b}$$

$$\psi^3(x,y)=\psi(x)\psi(y), \tag{9c}$$

$$\varphi(x,y)=\varphi(x)\varphi(y), \tag{9d}$$

where $\psi(x)$ and $\psi(y)$ are 1D wavelet functions, and $\varphi(x)$ and $\varphi(y)$ are 1D scaling functions, in the x- and y-directions, respectively. By dilating and translating mother wavelet and scaling functions, wavelet and scaling functions at the MRA level j can be obtained:

$$\psi^v_{j,k,l}(x,y)=2^{-j}\psi^v\left(2^{-j}x-k,2^{-j}y-l\right);j,k,l\in\mathbb{Z}, \tag{10a}$$

$$\varphi_{j,k,l}(x,y)=2^{-j}\varphi\left(2^{-j}x-k,2^{-j}y-l\right);j,k,l\in\mathbb{Z}. \tag{10b}$$

The signal of a discretized mode shape $W[x,y]$ can be decomposed into components at multiple levels:

$$W=\sum_j W_j. \tag{11}$$

Correspondingly, subspaces $\mathbf{W}_j$ of $\mathbf{L}^2(\mathbb{R})$ are spanned by $\psi^v_{j,k,l}$, which are orthogonal to each other; on the other hand, $\mathbf{V}_j$ can be spanned by $\psi^v_{i,k,l}$ for $i>j$, which leads to $\mathbf{V}_{j-1}=\mathbf{V}_j\oplus\mathbf{W}_j$, where

$$\mathbf{W}_j=\mathrm{span}\left(\psi^v_{j,k,l}:k,l\in\mathbb{Z}\right), \tag{12a}$$

$$\mathbf{V}_j=\mathrm{span}\left(\psi^v_{i,k,l}:k,l\in\mathbb{Z},i>j\right). \tag{12b}$$

Thus, $\mathbf{L}^2(\mathbb{R})$ can be decomposed as

$$\mathbf{L}^2(\mathbb{R})=\mathbf{V}_j\oplus\mathbf{W}_j\oplus\cdots\oplus\mathbf{W}_1\oplus\mathbf{W}_0\oplus\mathbf{W}_{-1}\oplus\mathbf{W}_{-2}\oplus\cdots \tag{13}$$

Accordingly, discrete W in $\mathbf{V}_0$ with the finest resolution can be decomposed into the approximation A_N in $\mathbf{V}_N$ and details D^v_j in $\mathbf{W}_j$:

$$W[x,y]=A_N[x,y]+\sum_{v=1}^{3}\sum_{j=1}^{N}D^v_j[x,y], \tag{14}$$

where A_N and D^v_j can be calculated by the DWT:

$$A_N=\sum_{v=1}^{3}\sum_{i>j}\sum_k\sum_l a^v_{i,k,l}\psi^v_{i,k,l}, \tag{15a}$$

$$D^v_j=\sum_k\sum_l a^v_{j,k,l}\psi^v_{j,k,l}, \tag{15b}$$

with wavelet transform coefficients $a^v_{j,k,l}$ being calculated by the inner product of W and $\psi^v_{j,k,l}$:

$$a^v_{j,k,l}=\langle W,\psi^v_{j,k,l}\rangle. \tag{16}$$

To formulate the MRTD, an appropriate wavelet needs to be selected. Among the Daubechies wavelet family, the Db 1 wavelet, also called the Haar wavelet, is employed in this study:

$$\varphi(x)=\begin{cases}1 & 0\le x<1,\\ 0 & \text{otherwise},\end{cases} \tag{17a}$$

$$\psi(x)=\begin{cases}1 & 0\le x<1/2,\\ -1 & 1/2\le x<1,\\ 0 & \text{otherwise}.\end{cases} \tag{17b}$$

The Haar wavelet is the simplest Daubechies wavelet with the first-order vanishing moment, which is easily accessible for most engineers.

By virtue of the first-order differentiating function of the DWT using the Haar wavelet, the wavelet coefficients $a^3_{j,k,l}$ by the 2D Haar DWT can be regarded as the second-order derivative of the mode shape W with respect to x and y at the level j. By further processing $a^3_{j,k,l}$ by the 2D Haar DWT, the new wavelet coefficients $a^{3*}_{j,k,l}$ can be regarded as the fourth-order derivative of W with respect to x and y at the level j, namely the MRTD, denoted as $T_{xy,j}$:

$$a^{3*}_{j,k,l}=\langle a^3_{j,k,l},\psi^3_{j,k,l}\rangle, \tag{18a}$$

$$T_{xy,j}[x,y]=a^{3*}_j[x,y]. \tag{18b}$$

By means of the MRA, noise involved in mode shapes during measurement can be largely eliminated at high levels. Thereby, the MRTD features higher robustness against noise interference than the twist derivative.

2.3. Damage index

To extract damage features from the MRTD, it is decomposed into components by singular value decomposition (SVD) [29]:

$$T_{xy,j}[x,y]=\sum_{r=1}^{R}T^r_{xy,j}[x,y]=\mathbf{U}_{m\times m}\mathbf{\Sigma}_{m\times n}\mathbf{V}^T_{n\times n}, \tag{19a}$$

$$T^r_{xy,j}[x,y]=\sigma_r\mathbf{u}_r\mathbf{v}^T_r, \tag{19b}$$

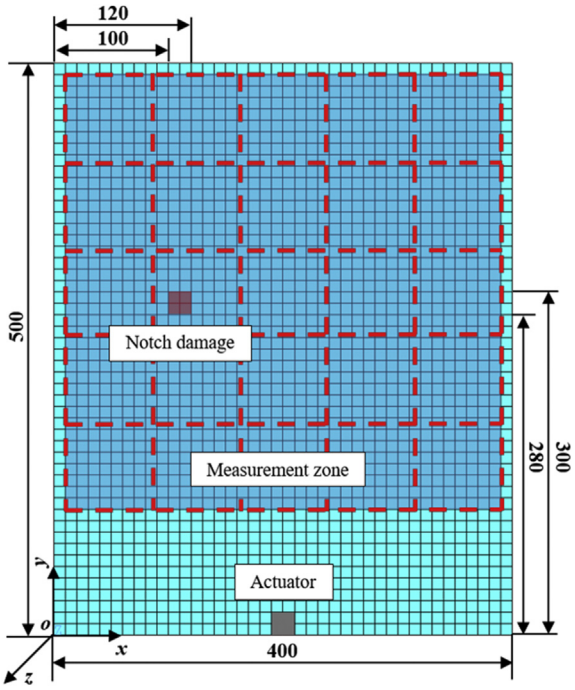

Fig. 1. FE model of the damaged plate (dimensions in millimeters) whose measurement zone consists of sub-regions (divided by red dashed lines).

where $T_{xy,j}$ is represented by an $m \times n$ matrix with the rank R and is decomposed into the $m \times m$ matrix $\mathbf{U} = \{\mathbf{u_1}, \mathbf{u_2}, ..., \mathbf{u_m}\}$, the $m \times n$ diagonal matrix $\mathbf{\Sigma}$ with singular values $\sigma_\mathbf{1}, \sigma_2, ..., \sigma_R$ in the descending order, and the $n \times n$ matrix $\mathbf{V} = \{\mathbf{v_1}, \mathbf{v_2}, ..., \mathbf{v_m}\}$. Among these components, the component $T^d_{xy,j}$ that is dominated by damage can be used as the damage index [30], denoted as DI:

$$DI[x, y] = T^d_{xy,j}[x, y]. \tag{20}$$

Damage-caused peaks in DI can represent damage-caused discontinuities in twist derivatives, by which the damage can be detected and localized. It is also worth mentioning that the approach proposed in this study for damage detection and localization of plate-type structures is model- and baseline-free, which means that geometrical and material parameters can be absent and no prior knowledge of mode shapes under the structurally intact status is required.

3. Numerical verification

The capability of the approach is numerically verified on a damaged plate by numerical simulation using the finite element (FE) method.

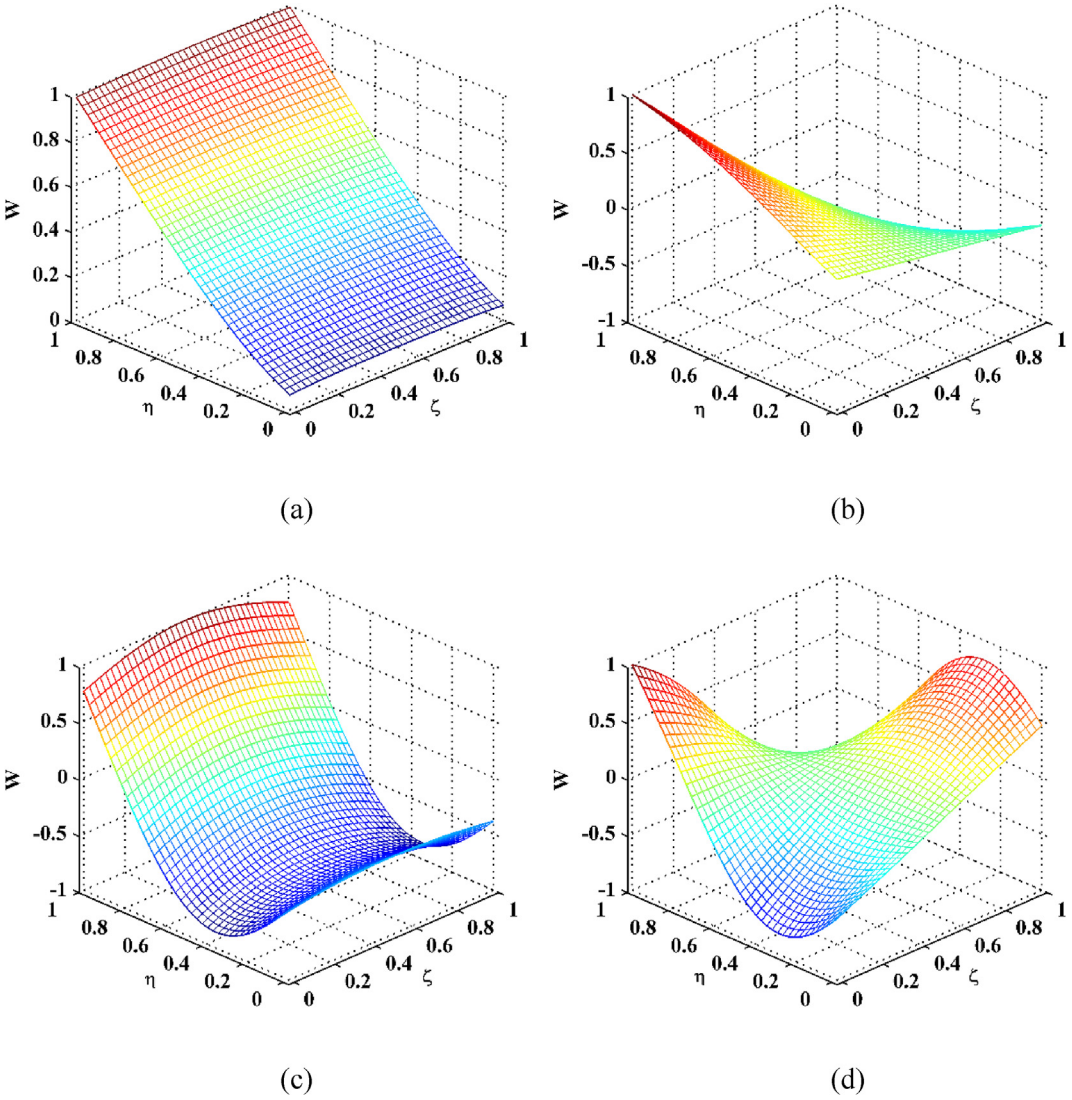

Fig. 2. The (a) first, (b) second, (c) third, and (d) fourth mode shapes of the damaged plate.

3.1. Numerical model of the damaged plate

A rectangular plate that bears a notch with reduced thickness in a square area is considered as the numerical specimen. The dimensions of the plate are 400 mm × 500 mm × 3 mm in the *x*-, *y*-, and *z*-directions, respectively. The lower edge of the plate is clamped and the other three edges are free. The plate is modeled by the FE software ANSYS using eight-node hexahedral elements whose dimensions are 10 mm × 10 mm × 1 mm in the *x*-, *y*-, and *z*-directions, respectively, as shown in Fig. 1. The elastic modulus, Poisson's ratio, and material density are 70.5 GPa, 0.33, and 2680 Kgm^{-3}, respectively. The notch damage is modeled by reducing one-third thickness in a square area (20 mm × 20 mm) from the front surface of the plate. The damage is centered at $x = 110$ mm and $y = 290$ mm. On the back surface of the plate, the measurement zone spans from $x = 10-390$ mm and from $y = 110-490$ mm. The damage area amounts to 0.277% of the measurement area. Without loss of generality, by introducing the dimensionless coordinates $\zeta = \frac{x}{380}$ and $\eta = \frac{y}{380}$, the notch is centered at $\zeta = 0.263$ and $\eta = 0.474$, spanning from 0.237 to 0.289 in ζ, and from 0.447 to 0.5 in η, respectively. A harmonic force of unit amplitude at a natural frequency is applied in the *z*-direction near the middle of the lower edge of the plate to simulate the transverse excitation generated by an actuator. By measuring steady-state responses from 39 × 39 nodes in the measurement zone, the operating deflection shape (ODS) of the plate with light damping can be obtained, which approximates the corresponding mode shape associated with the natural frequency.

Each group of 3 × 3 measurement points on the plate surface can depict the local deflection that can be assumed as a biquadratic function. Therefore, sparse sampling intervals in the measurement zone in the *x*- and *y*-directions can be about

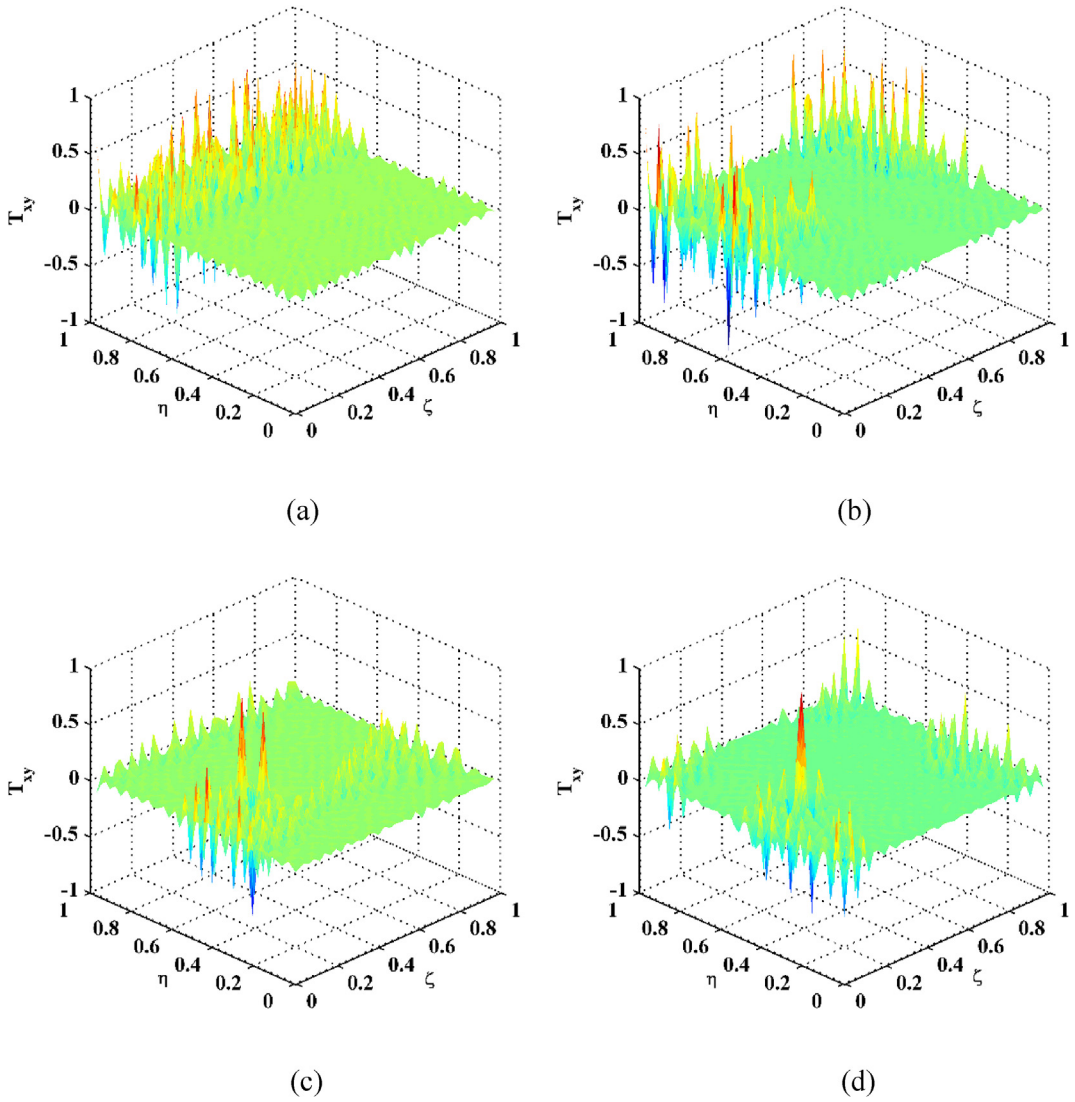

Fig. 3. Twist derivatives for the (a) first, (b) second, (c) third, and (d) fourth mode shapes.

half of the damage dimensions in the corresponding directions. Although denser sampling can provide higher resolution in mode shapes, it can be time-consuming for measurement and processing. With this concern, the sampling intervals are 10 mm in the x- and y-directions in this case. To compensate for the mode shape resolution for better visualization, bicubic interpolation [31] is implemented to increase dimensions of the mode shapes from 39×39 to 153×153. It is noteworthy that as dimensions of the damage are small, the sampling intervals need to be small enough to match the damage dimensions; on the other hand, the plate needs to be excited at high frequencies to produce short waves that match the small damage.

3.2. Numerical results

(1) Choice of mode shapes

The first several modes can be more easily obtained than higher modes; nevertheless, they lack adequate sensitivities to small damage [7]. The first four out-of-plane mode shapes W of the plate are obtained by ANSYS and shown in Fig. 2, whose twist derivatives T_{xy} are calculated by Eq. (8) and shown in Fig. 3. It can be seen from Fig. 3(a) and (b) that only some burrs appear at locations where amplitudes in the corresponding mode shapes are large, whereas any damage-caused peak can be barely recognized. These burrs are induced by errors in the FE calculation and amplified by the finite difference method. In Fig. 3(c) and (d), the damage-caused peaks can be recognized but ambiguous for damage identification, because the third and fourth mode shapes become more fluctuant as shown in Fig. 3(c) and (d), respectively. By addressing the inadequate sensitivities of lower modes to small damage, higher modes are used in this study.

It is well known that sensitivities of mode shapes to damage depend on the damage location: damage close to nodal lines can barely cause changes in derivatives of mode shapes, whereas damage near local fluctuant deformations can cause noticeable changes. Thereby, mode shapes with local large amplitudes in the vicinity of the damage is beneficial for detecting damage. However, the approximate location of damage is unknown and it is time-consuming to find appropriate mode

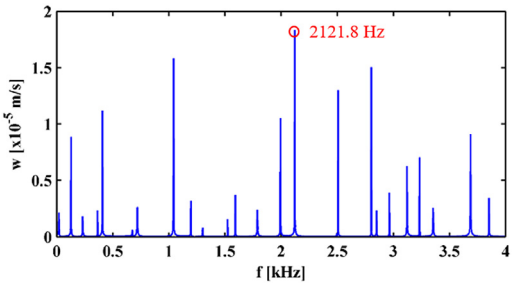

Fig. 4. Frequency spectrum of the central displacement of the sub-region without damage.

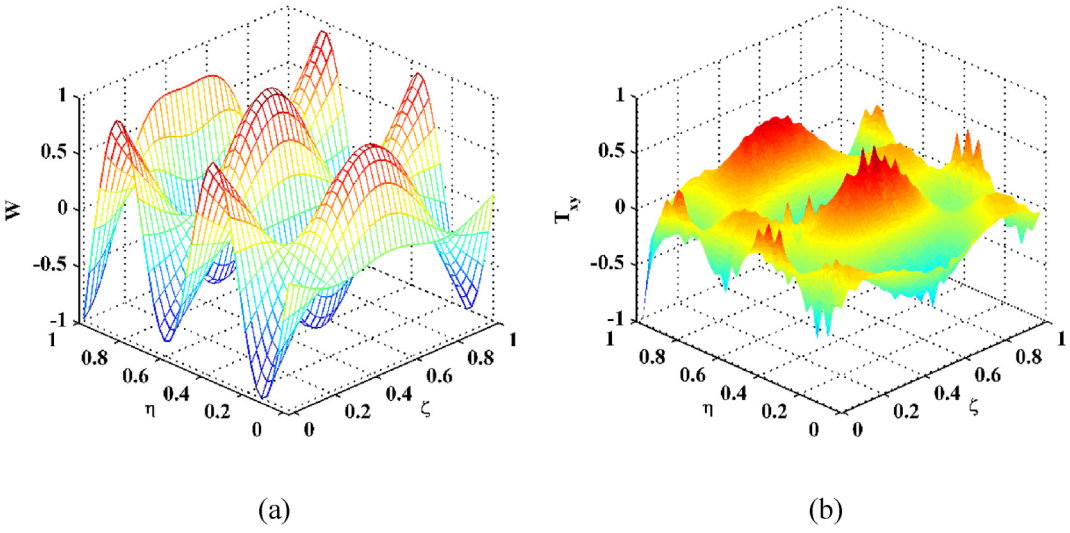

Fig. 5. (a) Mode shape at 2121.8 Hz and (b) its twist derivative.

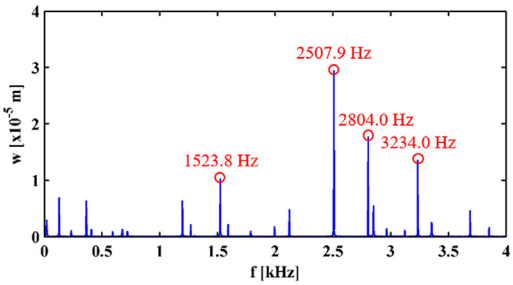

Fig. 6. Frequency spectrum of the central displacement of the sub-region with the damage.

shapes by searching a large number of modes one by one. By addressing this problem, this study proposes a strategy of collecting candidate modes from sub-regions in the measurement zone: first, the measurement zone is divided into several small sub-regions; then, the plate is excited by the sweeping force in a wide frequency range, and meanwhile the time history of vibration at each sub-region center is individually measured; then, in each frequency spectrum, the candidate mode for

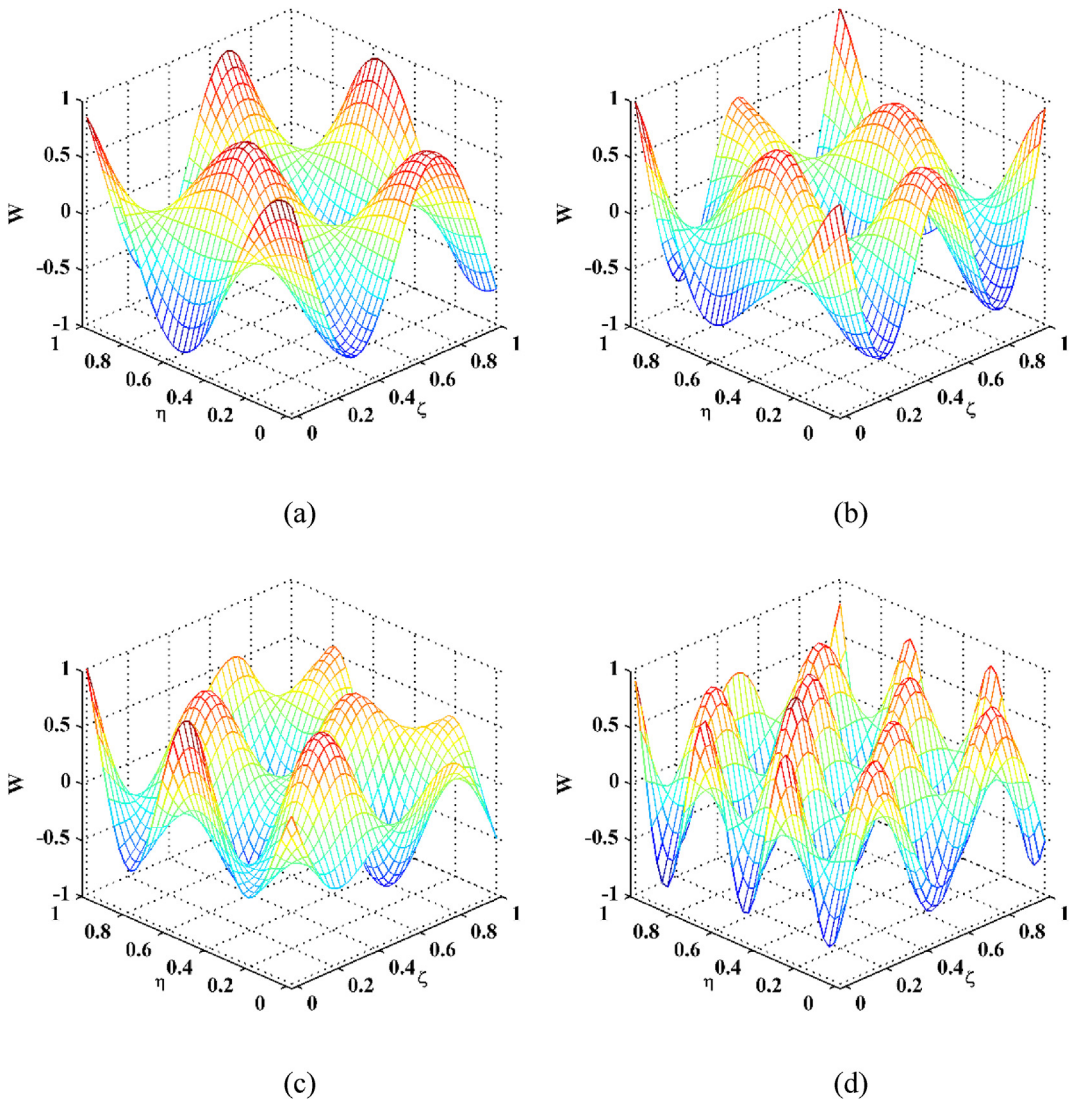

Fig. 7. Mode shapes for Scenarios (a) I, (b) II, (c) III, and (d) IV.

each sub-region is selected by finding the natural frequency with the largest amplitude; and finally, the mode shape that is most sensitive to the damage can be chosen from these candidate modes after trials. It is noteworthy that the exact mode numbers of selected candidate modes can be unknown.

The measurement zone shown in Fig. 1 is divided into 5×5 sub-regions indicated by red dashed lines. The plate is excited by the harmonic force with the sweeping frequency from 0 to 4 kHz. The displacement at the center of each sub-region is simultaneously obtained. Sensitivities of selected candidate modes depend on the sub-regions they belong to; thereby candidate modes for sub-regions without the damage can be less or not sensitive to the damage. Consider a sub-region without the damage, spanning from 0.6 to 0.8 in ζ, and from 0.6 to 0.8 in η. The frequency spectrum of its central displacement is shown in Fig. 4, where the natural frequency with the largest amplitude is 2121.8 Hz. The corresponding normalized mode shape is obtained with its maximum amplitude being unit, as shown in Fig. 5(a). Accordingly, its T_{xy} is obtained by Eq. (8) and shown in Fig. 5(b). For generality, T_{xy} is also normalized with its maximum amplitude being unit. No evident damage-caused peak in T_{xy} appears to indicate the presence of the damage. In this case, the candidate mode for the sub-region without damage lacks the capability of detecting damage.

The frequency spectrum of the central displacement of the sub-region with damage is shown in Fig. 6. To verify the capability and robustness of the approach, more than one mode shapes are used in this case. The natural frequencies of 1523.8, 2507.9, 2804.0, and 3234.0 Hz with the first four largest amplitudes are selected, labeled as Scenarios I, II, III, and IV,

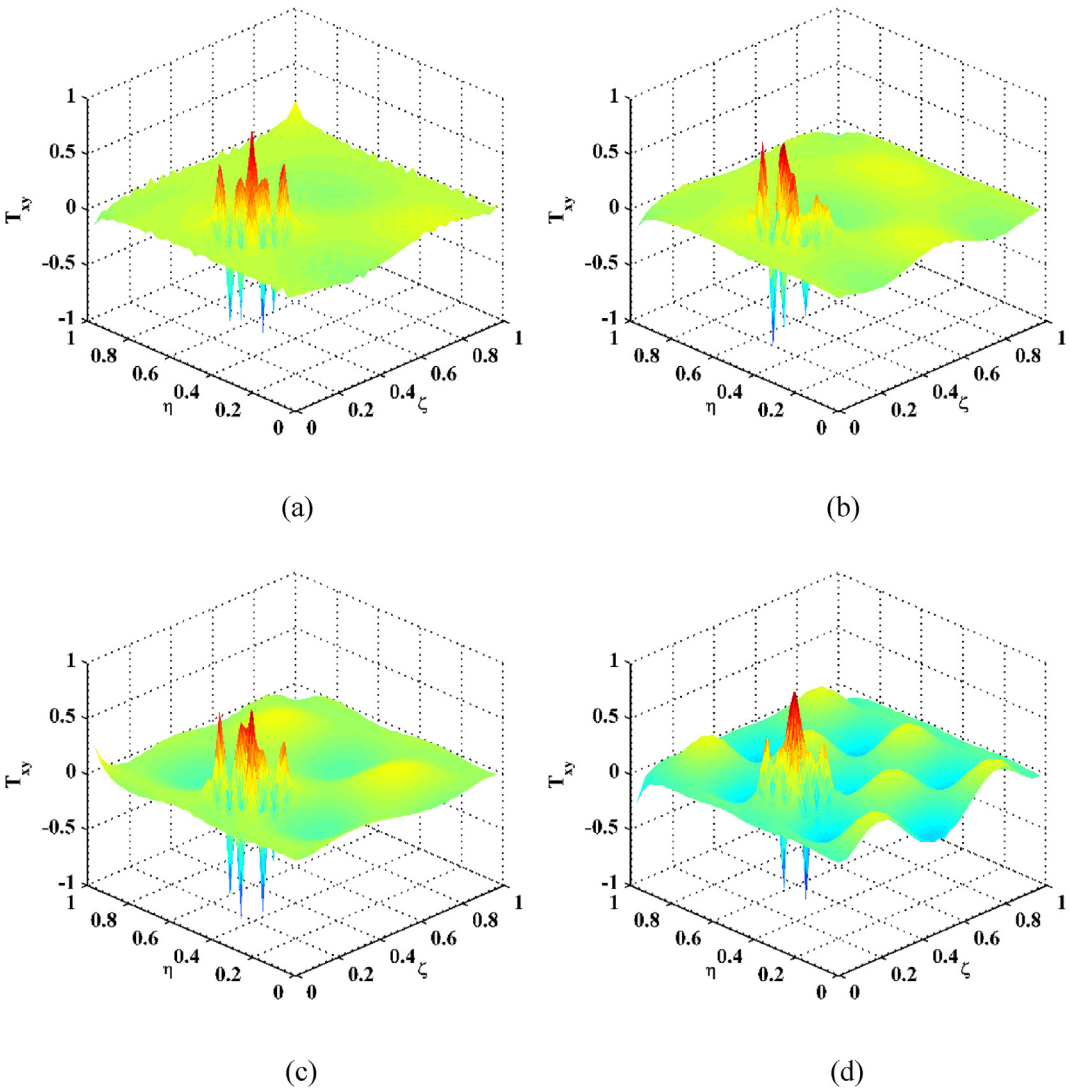

Fig. 8. Twist derivatives for Scenarios (a) I, (b) II, (c) III, and (d) IV.

respectively. The corresponding normalized mode shapes are obtained and shown in Fig. 7. By Eq. (8), the twist derivatives T_{xy} are obtained from the mode shapes and shown in Fig. 8. In each T_{xy}, a main peak appears in the damage region; around the main peak, several side peaks with smaller amplitudes also appear in the vicinity of the damage region. Thereby, the presence of the damage can be evidently manifested.

(2) Robustness against noise interference

In a real scenario, noise components are inevitably involved in the measured mode shapes. With this concern, Gaussian white noise is incorporated into the noise-free mode shapes, whereby the noisy mode shapes with the signal-to-noise ratio of 60 dB are produced. The corresponding T_{xy} are obtained by Eq. (8) and shown in Fig. 9. It can be seen in Fig. 9 that due to the differentiation in Eq. (8), noise interference is amplified, making the damage-induced discontinuity peaks become ambiguous.

To eliminate noise interference in the twist derivatives, the MRA is applied according to Eq. (18b), by which the MRTDs are formulated. For Scenario I, by means of gradually increasing the MRA level from 20 to 50, the corresponding MRTDs are obtained and shown in Fig. 10. Each $T_{xy,j}$ is normalized with the maximum amplitude being unit. It is noteworthy that values of $T_{xy,j}$ near boundaries of the plate are made to vanish, in order to remove the intrinsic boundary effect in the DWT [7,32]. It can be seen from Fig. 10 that noise interference is gradually eliminated with the increase of the MRA level; meanwhile, the damage-caused peaks are retained to clearly indicate the damage. The MRTD $T_{xy,50}$ in Fig. 10(d) is smooth enough, which

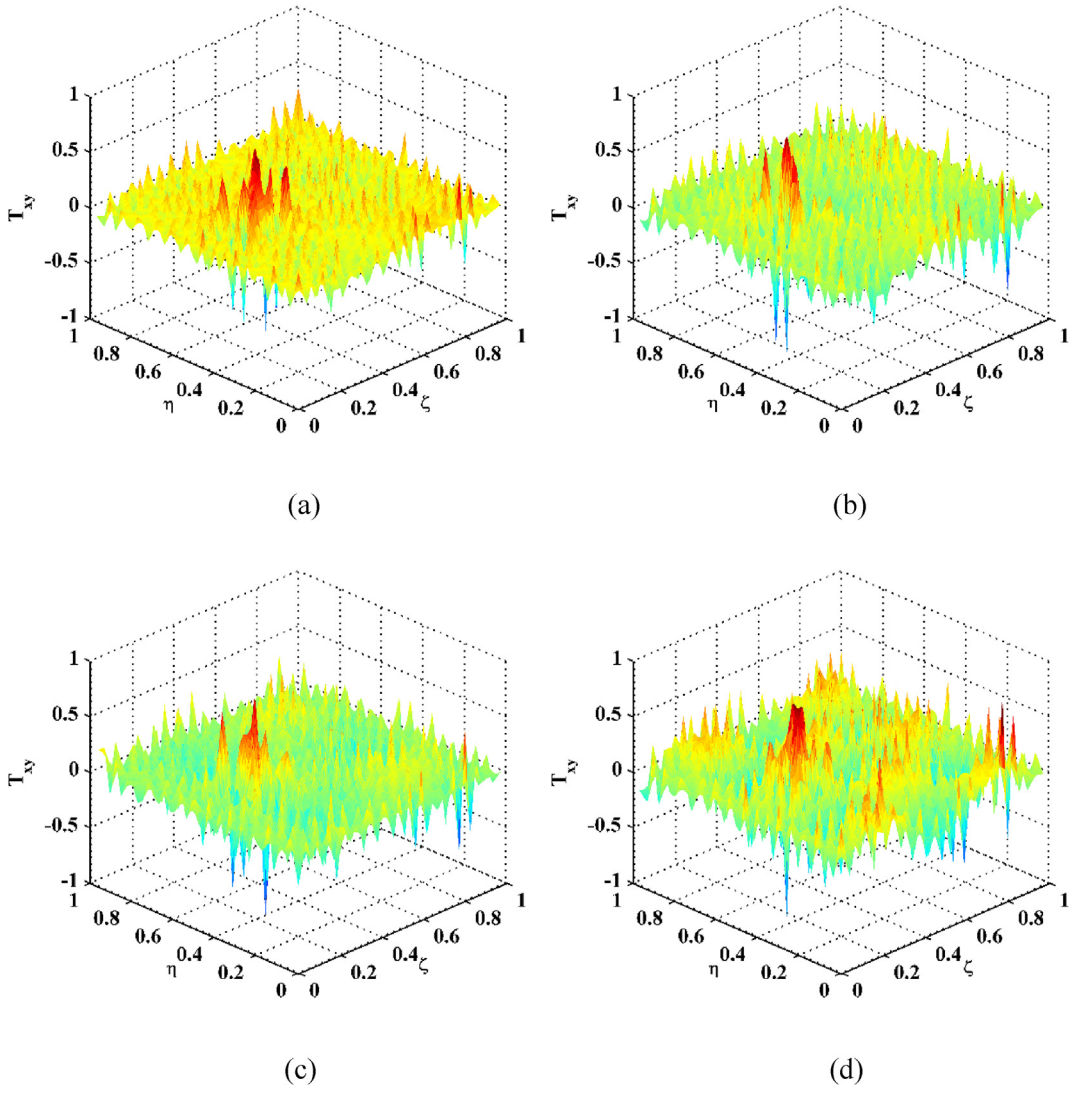

Fig. 9. Twist derivatives for Scenarios (a) I, (b) II, (c) III, and (d) IV with noise interference.

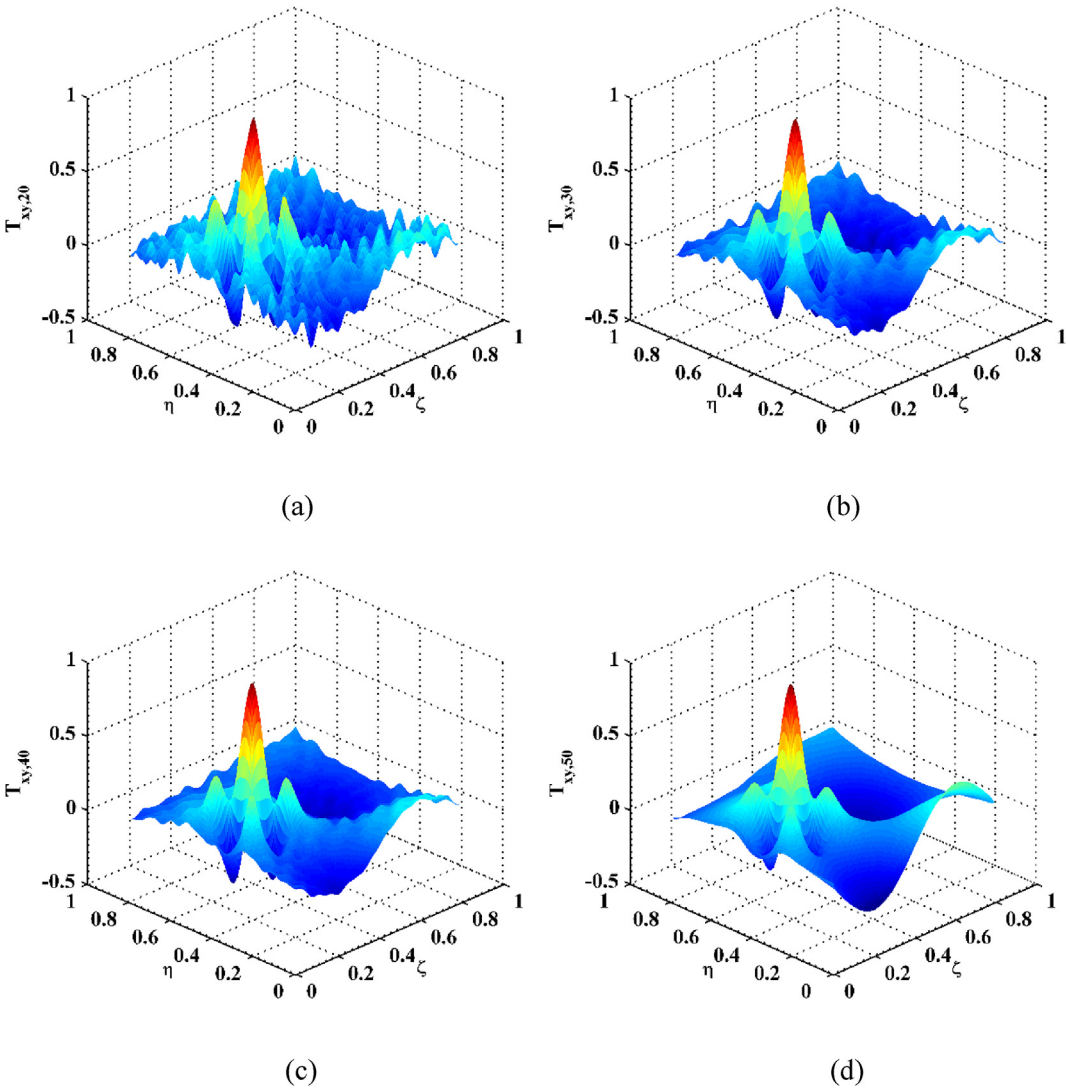

Fig. 10. MRTDs for Scenario I at MRA levels of (a) 20, (b) 30, (c) 40, and (d) 50.

means that most of noise components have been eliminated. The MRTDs $T_{xy,50}$ for Scenarios I through IV are calculated and shown in Fig. 11, where noise interference in each scenario is basically eliminated. The damage-caused main and side peaks in $T_{xy,50}$ can be evidently recognized in Fig. 11. Thereby, the satisficing MRA level in this case is 50. Nevertheless, the global trends in $T_{xy,50}$ obscure the damage-caused peaks for clearly characterizing the damage.

(3) Detection and localization of damage

By Eq. (19), $T_{xy,50}$ is decomposed into components by SVD, among which the second component $T^2_{xy,50}$ is found to be the component dominated by the damage. Accordingly, damage indices *DI* are obtained by Eq. (20), as shown in Fig. 12(a), (b), (c), and (d) for Scenarios I, II, III, and IV, respectively. It can be seen from Fig. 12 that the global trends are totally removed and only the damage-caused main and side peaks are retained. Thereby, the damage can be detected and localized by the main peaks. To clearly show the main peaks, *DI* is multiplied by a dimensionless threshold of 0.6 after several trials, whose planforms are shown in Fig. 13. It can be seen in Fig. 13 that for each scenario the location and size of the damage are well characterized by the main peaks: the detected damage is centered at about $\zeta = 0.265$ and $\eta = 0.475$, spanning from about 0.24 to 0.29 in ζ, and 0.45 to 0.5 in η, respectively, corresponding to the actual location and size of the notch.

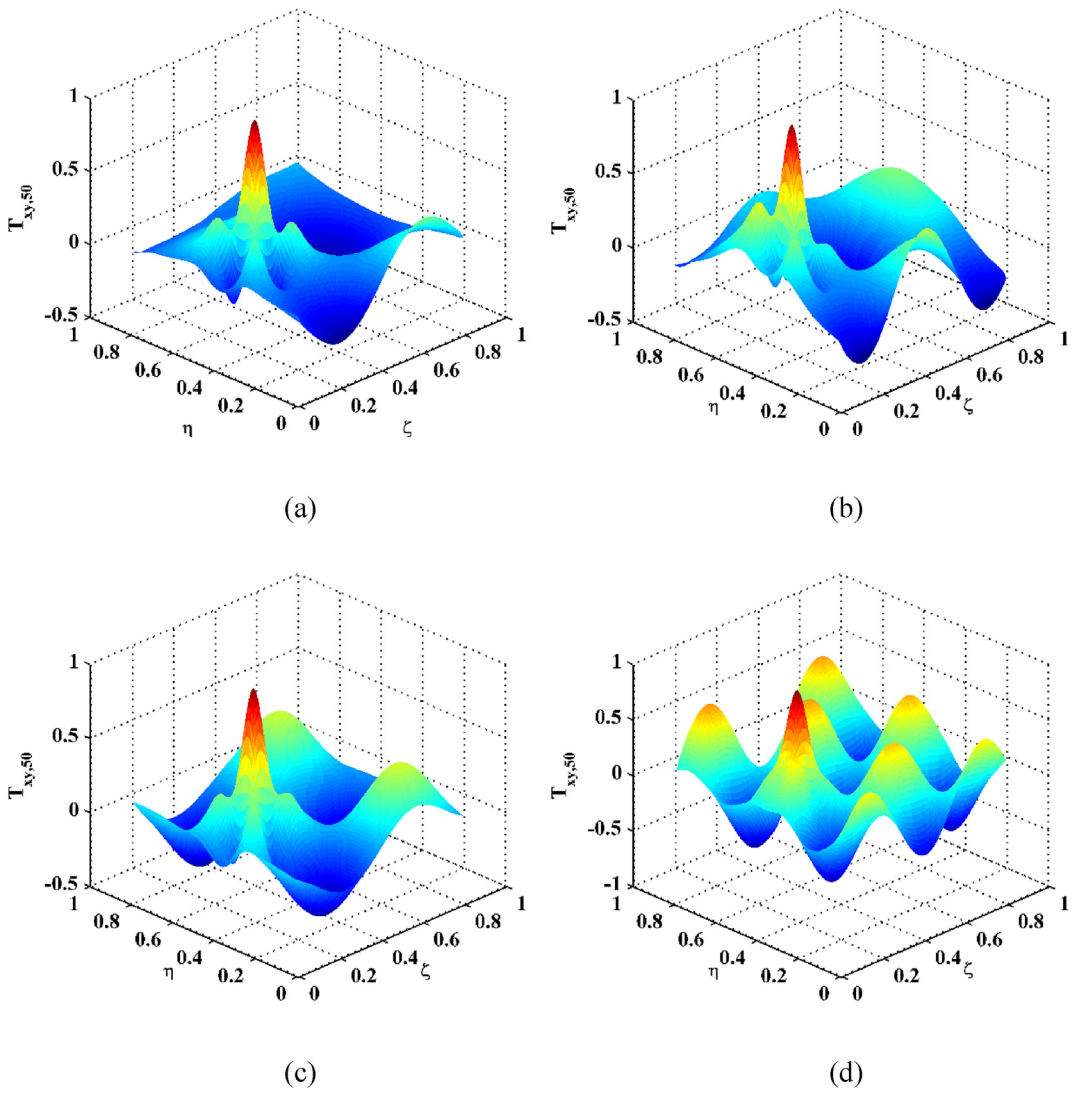

Fig. 11. MRTDs for Scenarios (a) I, (b) II, (c) III, and (d) at the MRA level of 50.

(4) Effect of sampling intervals

To investigate the effect of sampling intervals on the approach in characterizing damage, Scenario IV associated with smaller sampling intervals (one quarter of damage dimensions in both the *x*- and *y*-directions) is considered as Scenario V. The mode shape for Scenario V is shown in Fig. 14(a), whose planform of *DI* in Fig. 14(b) clearly characterizes the location and size of the damage. As shown in Figs. 13(d) and 14(b), the detected damage for Scenarios IV and V with different sampling intervals is almost the same. Scenario V with smaller damage is considered as Scenario VI, in which the damage dimensions are reduced by half, *i.e.*, 10 mm × 10 mm. Accordingly, sampling intervals are reduced by half, *i.e.*, 5 mm in the *x*- and *y*-directions. The mode shape for Scenario VI is shown in Fig. 15(a) with its planform of *DI* shown in Fig. 15(b), in which the damage location and size can be clearly characterized. Thereby, half of the damage dimensions can be regarded as satisficing sampling intervals for damage detection and localization of plate-type structures.

4. Experimental validation

The applicability of the approach is experimentally validated by detecting damage in a rectangular plate through non-contact measurement using a SLV, which was implemented in the Structural Dynamics Laboratory at Hohai University.

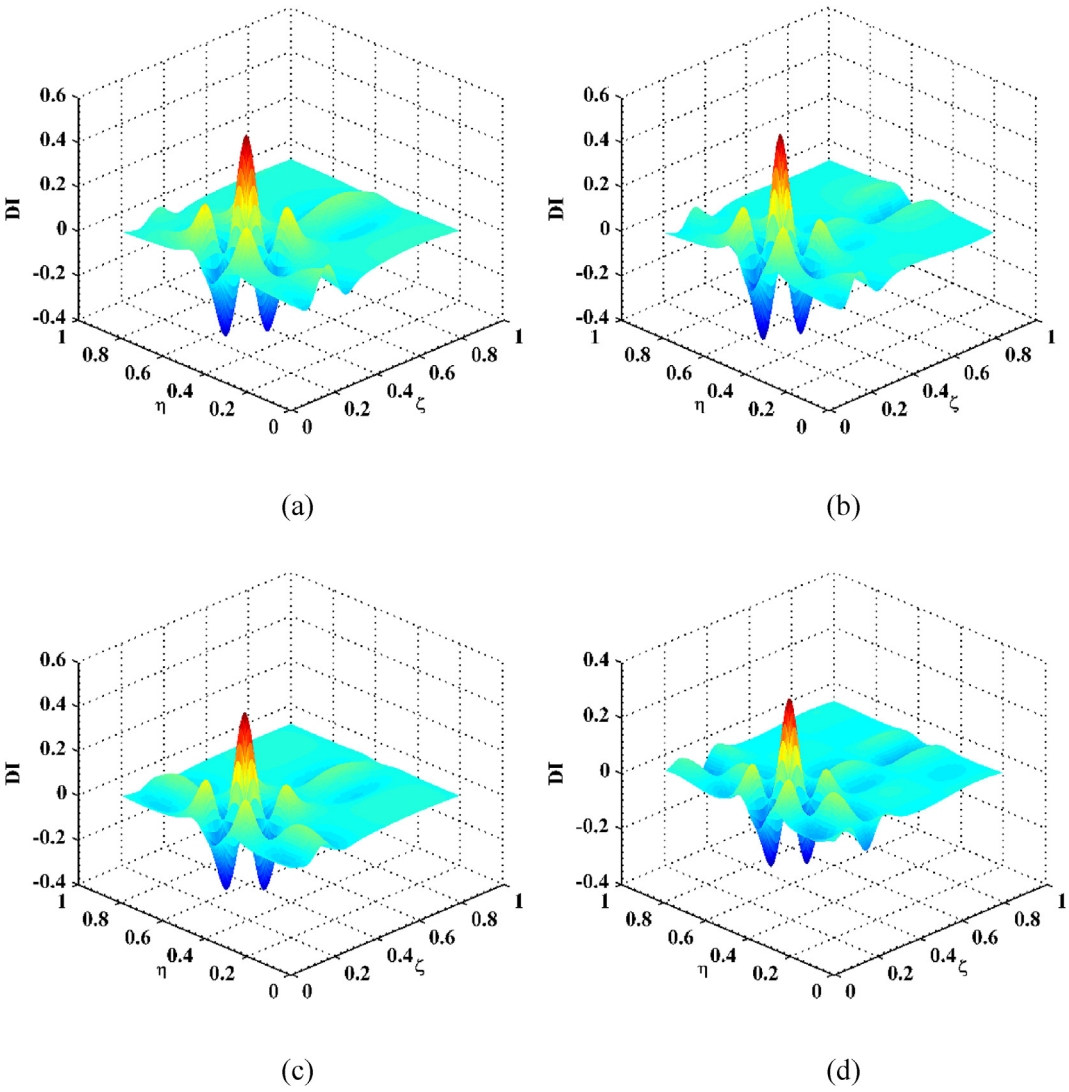

Fig. 12. Damage indices for Scenarios (a) I, (b) II, (c) III, and (d) IV.

4.1. Experimental specimen of the damaged plate

The material of the plate specimen is Aluminum 6061. The dimensions of the plate are 400 mm × 600 mm × 3 mm in width, height, and thickness, respectively. The lower part of the plate with 100 mm in height is clamped as shown in Fig. 16. A notch damage was manufactured by digging one-third thickness in a square area (20 mm × 20 mm) from the front surface. The experimental specimen is shown in Fig. 16, where the measurement zone (380 mm × 380 mm) on the back surface is marked in blue. Dimensions and locations of the measurement zone and notch damage are exactly the same as those in the numerical model used in Section 3. A square PZT actuator (50 mm × 50 mm × 1 mm) is placed near the middle of the lower edge of the plate to generate transverse harmonic excitations. Zoomed-in views of the notch damage and PZT actuator on the front surface are also shown in Fig. 16. The PZT actuator (PZT-4) is custom-manufactured by Hanzhou Technology Co. in China, whose resonance frequency in the thickness direction is about 2 MHz. Its frequency range starts from 0 Hz up to the MHz level, depending on structures excited by the actuator. The experimental set-up is shown in Fig. 17. A SLV (Polytec PSV-400) is employed to scan the entire measurement zone on the back surface of the plate with 39 × 39 uniformly-distributed measurement points whose intervals are 10 mm in the *x*- and *y*-directions, in accord with the sparse sampling in the numerical simulation. The velocity decoder of the SLV is Polytec VD-02 for a velocity up to 10 m/s and a frequency up to 1.5 MHz. Displacement/velocity/acceleration responses of 39 × 39 measurement points in the measurement zone are acquired by the SLV, whereby the displacement ODSs are obtained. When the plate with light damping is excited at a natural frequency, the

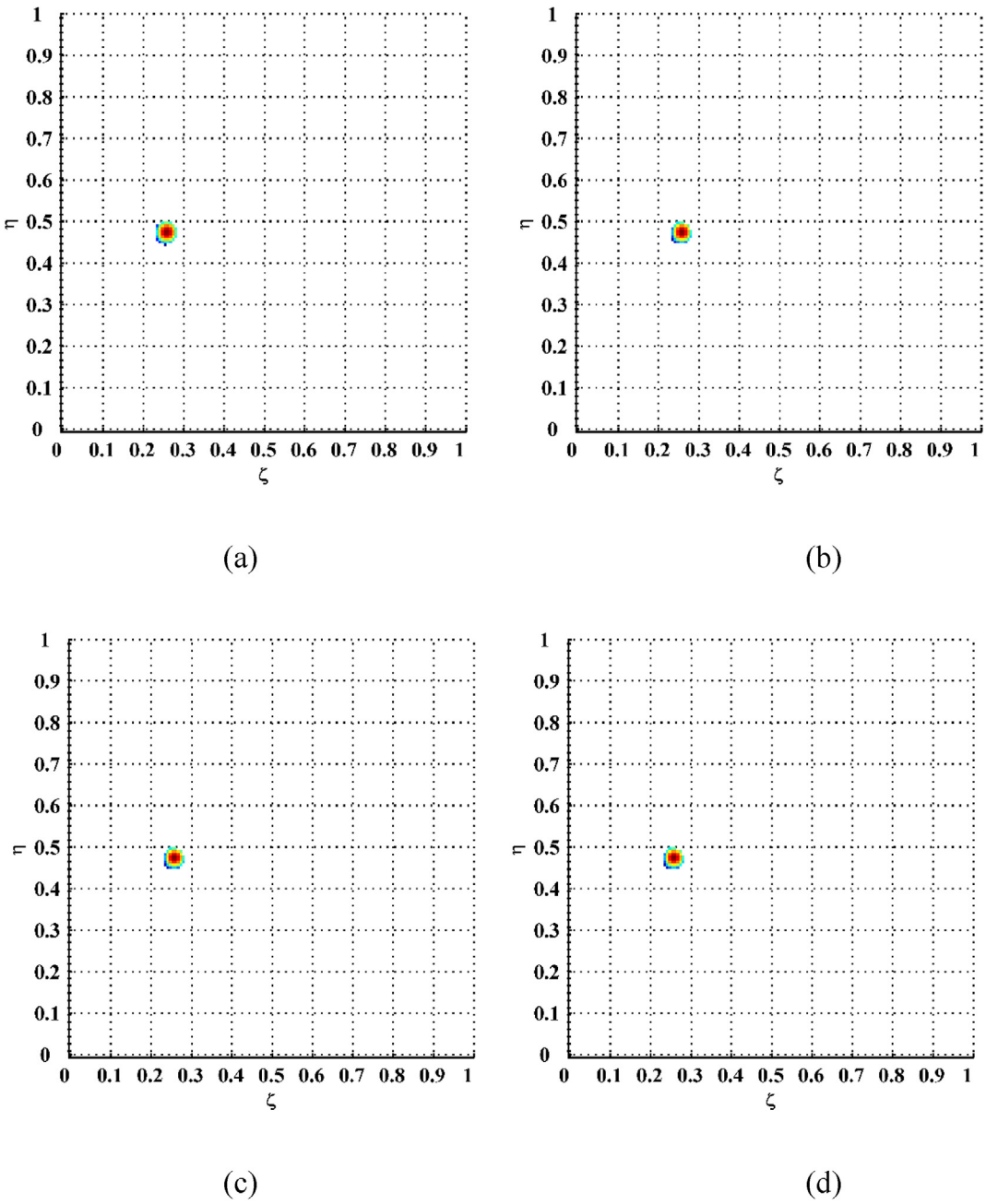

Fig. 13. Planforms of damage indices for Scenarios (a) I, (b) II, (c) III, and (d) IV.

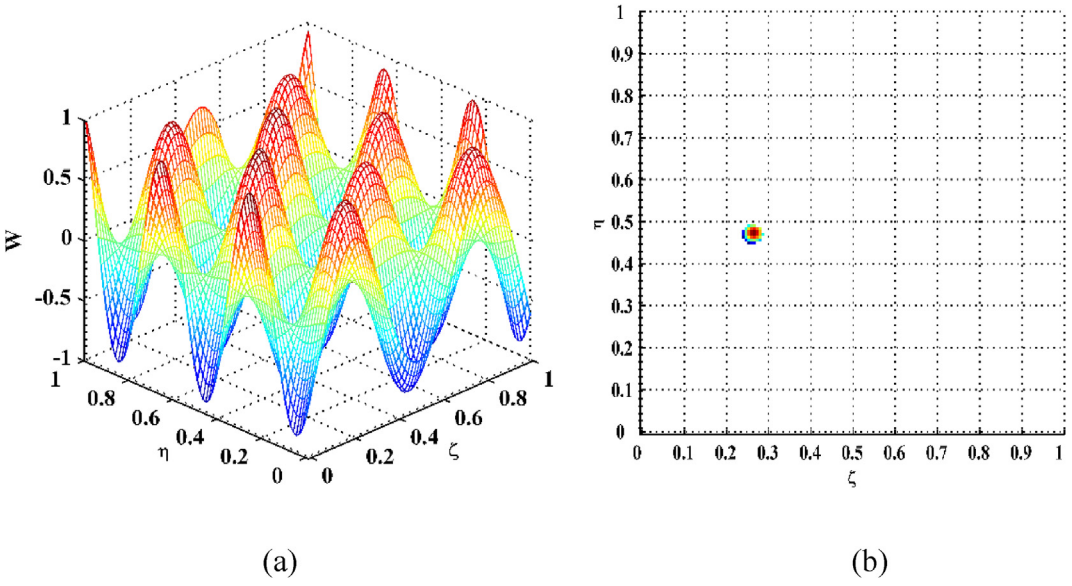

Fig. 14. (a) Mode shape for Scenario V and (b) the planform of the damage index.

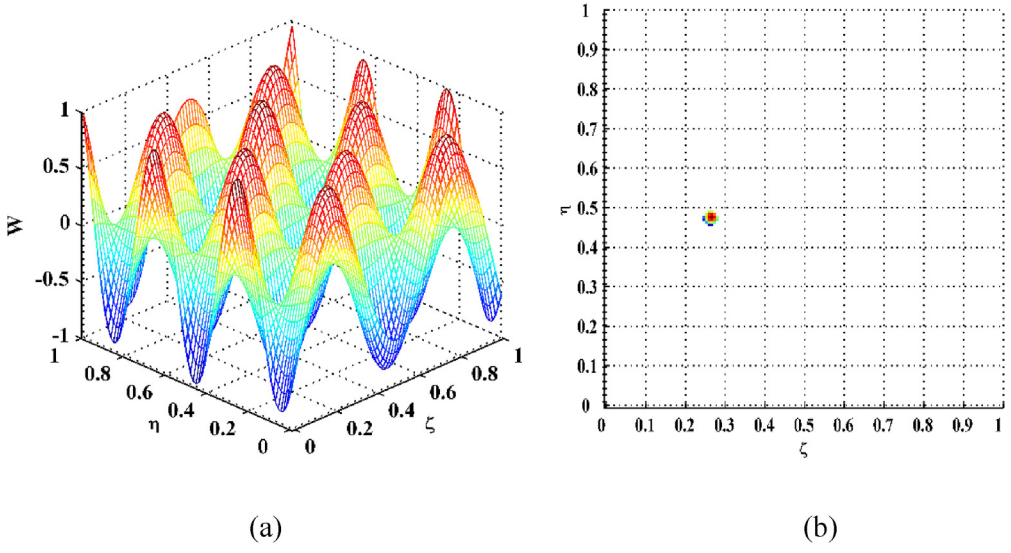

Fig. 15. (a) Mode shape for Scenario VI and (b) the planform of the damage index.

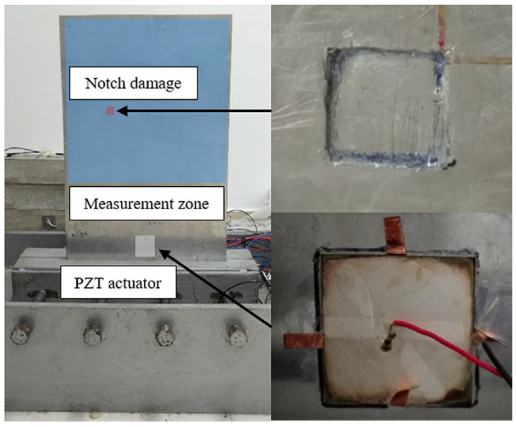

Fig. 16. Experimental specimen: the damaged plate with a PZT actuator attached to it.

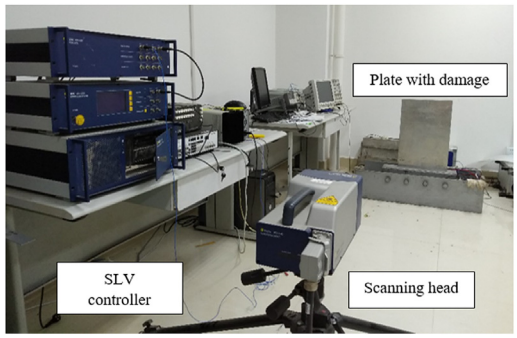

Fig. 17. Experimental set-up: a SLV system.

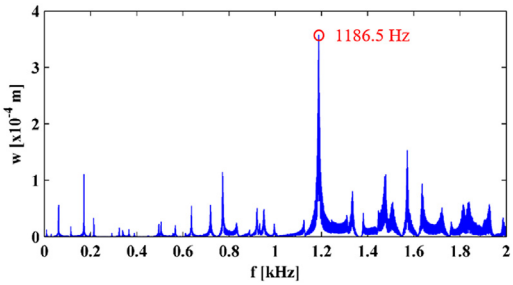

Fig. 18. Frequency spectrum of the central displacement of the sub-region with the damage.

ODS approximates the corresponding mode shape. Bicubic interpolation is implemented to increase the dimensions of the measured mode shapes from 39 × 39 to 153 × 153.

4.2. Experimental results

In accord with the numerical simulation, the measurement zone of the plate is divided into 5 × 5 sub-regions. The plate is excited by the harmonic force generated by the PZT actuator with the sweeping frequency from 0 to 2 kHz. Simultaneously,

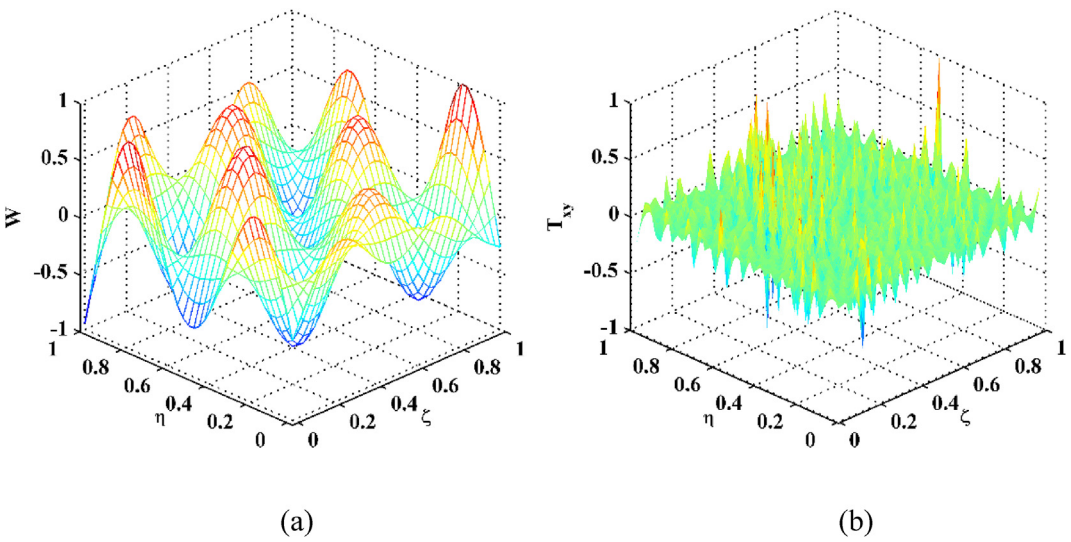

Fig. 19. (a) Mode shape of the damaged plate and (b) its twist derivative.

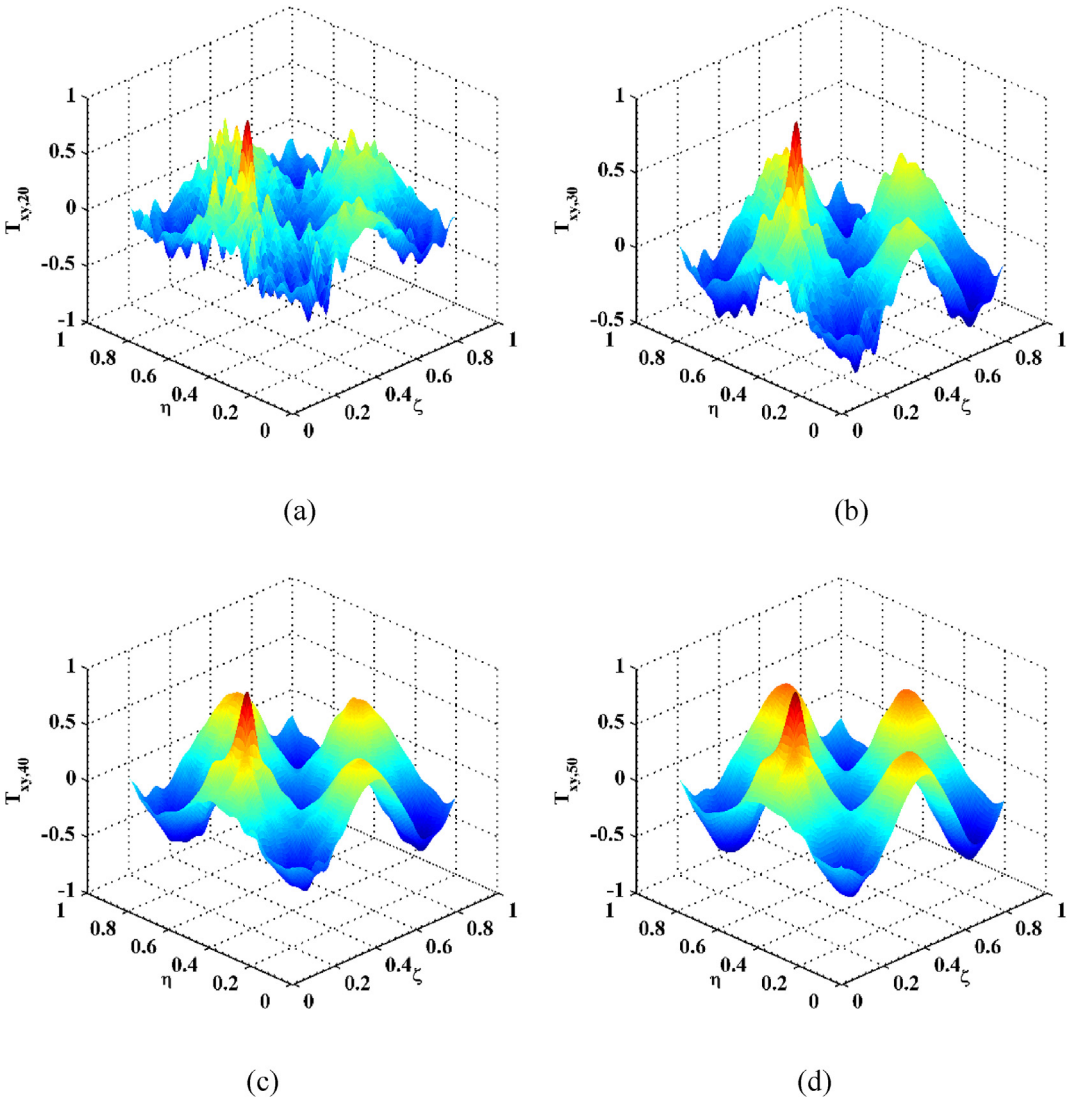

Fig. 20. MRTDs at MRA levels of (a) 20, (b) 30, (c) 40, and (d) 50.

central displacement responses of the sub-regions are individually acquired through non-contact laser measurements using the SLV. In their frequency spectra, candidate modes for all sub-regions are determined by finding the natural frequencies with largest amplitudes. Among the 25 selected candidate modes, the mode shape associated with the natural frequency of 1186.5 Hz is found to be most sensitive to the damage. This mode is selected from the frequency spectrum of the central displacement of the sub-region with the damage, as shown in Fig. 18. For the ODS at the natural frequency of 1186.5 Hz, its real part has a larger amplitude than the imaginary part; it is thereby used as the corresponding mode shape [33]. The normalized mode shape W is shown in Fig. 19(a), from which the normalized twist derivative T_{xy} is obtained by Eq. (8) and shown in Fig. 19(b). It can be seen that noise interference dominates the twist derivative, masking any damage-caused peak that can indicate the presence of the damage. By Eq. (18b), the twist derivative is transformed to the MRTD, in which noise interference can be gradually eliminated by increasing the MRA level; meanwhile, the damage-caused peaks are retained to clearly indicate the damage. It can be found in Fig. 20 that up to the MRA level of 50, noise interference is basically eliminated in $T_{xy,50}$. Thereby, the satisficing MRA level in this case is 50.

By Eq. (19), $T_{xy,50}$ is decomposed into components by SVD, among which the second component $T^2_{xy,50}$ is found to be the component dominated by the damage. The damage index DI is obtained by Eq. (20) and shown in Fig. 21(a), where the damage-caused peaks evidently manifest the presence of the damage. In its planform shown in Fig. 21(b) with the dimensionless threshold of 0.6, the location and size of the damage are clearly characterized by the main peak: the detected damage

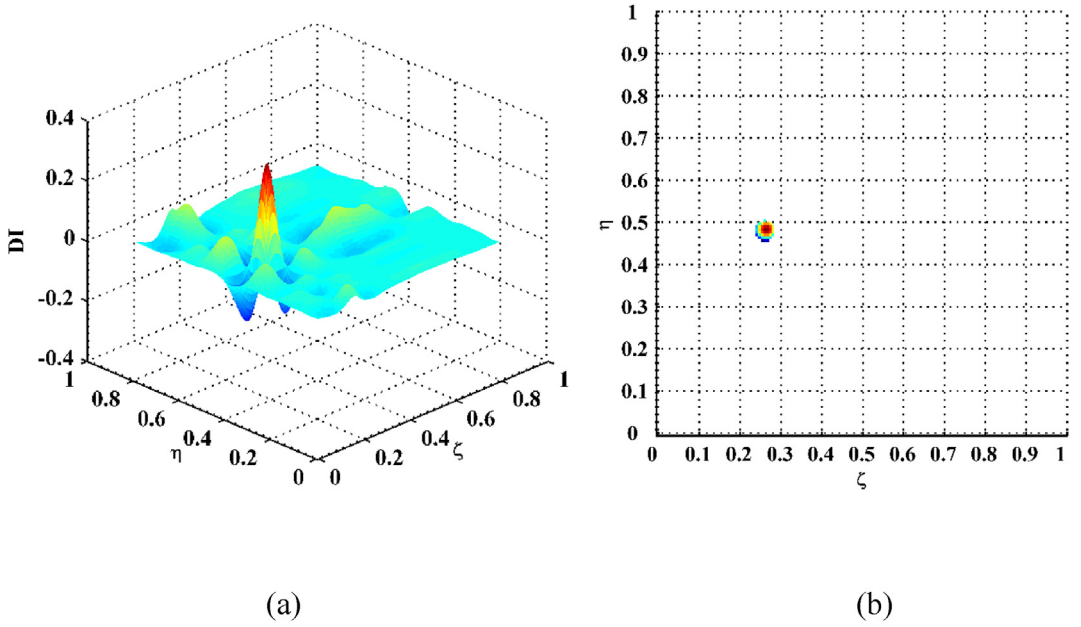

Fig. 21. (a) Damage index and (b) its planform.

is centered at about $\zeta = 0.265$ and $\eta = 0.475$, spanning from about 0.24 to 0.29 in ζ, and 0.45 to 0.5 in η, respectively, in good agreement with the actual location and size of the notch.

Methods of damage identification of real-world structural components that rely on laser scanning can encounter some difficulties in industrial applications, such as cost and agility of portage of a SLV and accessibility to structural components that are not easy to inspect. By addressing these problems, Park et al. [34] discussed the applicability of laser scanning to detection of delamination in wind turbine blades. A SLV can be carried on a vehicle to inspect real structural components because of its long-range inspection of up to tens of meters. For structural components at locations that are not easy to inspect directly, mirrors can be used to reflect laser beams from the SLV, so that laser beams can scan on the surfaces of the inspected components. Applications of the proposed approach to real-world structural components can be addressed in some future study.

5. Concluding remarks

Among vibration-based damage detection methods for plate-type structures, approaches relying on derivatives of out-of-plane mode shapes through non-contact laser scanning measurement have become a research focus during the recent decade. This study addresses the physical sense of twist derivatives in reflecting damage-caused discontinuities in shear strains, based on which a novel damage index is established for detecting and locating damage in plate-type structures. In particular, a strategy of choosing mode shapes and a scheme of sparsely sampling them are proposed. The capability of the proposed approach is numerically verified by FE simulation and experimentally validated through laser scanning measurement. The results show that the novel damage index can accurately characterize the presence, location, and size of the damage, and is robust against noise interference. Some conclusions are as follows.

(1) In a physical sense, damage can cause discontinuities in shear strains; conversely, such discontinuities can be reflected in twist derivatives of mode shapes, whereby the presence of the damage can be manifested.
(2) By integrating the MRA into the twist derivative, a new concept of MRTD is formulated with high robustness against noise interference, based on which the damage index is established using SVD. The location and size of the damage can be characterized by the damage index.
(3) With the objective of finding appropriate mode shapes that are sensitive to small damage, a strategy of collecting candidate modes from sub-regions is proposed in this study. The mode shape that is most sensitive to the damage can be chosen from these candidate modes after trials.
(4) A scheme of sparsely sampling mode shapes is proposed in this study. Half of damage dimensions can be regarded as satisficing sampling intervals for damage detection and localization of plate-type structures. To compensate for the mode shape resolution for better visualization, bicubic interpolation is implemented to increase dimensions of the mode shapes.

Declaration of competing interest

The authors declare that they have no known competing financial interests or personal relationships that could have appeared to influence the work reported in this paper.

CRediT authorship contribution statement

Wei Xu: Methodology, Software, Validation, Writing - original draft. **Weidong Zhu:** Conceptualization, Funding acquisition, Writing - review & editing. **Maosen Cao:** Methodology. **Hao Wu:** Validation. **Ruihu Zhu:** Validation.

Acknowledgements

The corresponding author Weidong Zhu is grateful for the support from the National Science Foundation through Grant No. CMMI-1763024. The co-authors Wei Xu and Ruihu Zhu are grateful for the support from the National Natural Science Foundation of China through Grant Nos. U1765204 and 51709093, respectively. The co-author Hao Wu did the experiment in the Structural Dynamics Laboratory at Hohai University with his former colleague Binkai Shi who also prepared the specimen.

References

[1] Z. Su, L. Ye, Y. Lu, Guided Lamb waves for identification of damage in composite structures: a review, J. Sound Vib. 295 (2006) 753–780.
[2] D. Chetwynd, J.A. Rongong, S.G. Pierce, K. Worden, Damage detection in an aluminium plate using outlier analysis, Fatig. Fract. Eng. Mater. Struct. 31 (8) (2008) 629–643.
[3] D. Garcia, R. Palazzetti, I. Trendafilova, C. Fiorini, A. Zucchelli, Vibration-based delamination diagnosis and modelling for composite laminate plates, Compos. Struct. 130 (2015) 155–162.
[4] A. Shelke, T. Kundu, U. Amjad, K. Hahn, W. Grill, Mode-selective excitation and detection of ultrasonic guided waves for delamination detection in laminated aluminum plates, IEEE Trans. Ultrason. Ferroelectrics Freq. Contr. 58 (3) (2011) 567–577.
[5] W. Ostachowicz, M. Radzieński, M. Cao, W. Xu, Novel technique for damage detection based on mode shape analysis, in: Vibration-Based Techniques for Damage Detection and Localization in Engineering Structures, World Scientific Publishing, 2018.
[6] M. Rucka, K. Wilde, Application of continuous wavelet transform in vibration based damage detection method for beams and plates, J. Sound Vib. 297 (2006) 536–550.
[7] W. Fan, P. Qiao, A 2-D continuous wavelet transform of mode shape data for damage detection of plate structures, Int. J. Solid Struct. 46 (25–26) (2009) 4379–4395.
[8] M.S. Cao, H. Xu, R.B. Bai, W. Ostachowicz, M. Radzieński, L. Chen, Damage characterization in plates using singularity of scale mode shapes, Appl. Phys. Lett. 106 (2015) 121906.
[9] B. Shi, P. Qiao, A new surface fractal dimension for displacement mode shape-based damage identification of plate-type structures, Mech. Syst. Signal Process. 103 (2018) 139–161.
[10] S. Timoshenko, S. Woinowsky-Krieger, Theory of Plates and Shells, McGraw-Hill, 1959.
[11] P. Qiao, K. Lu, W. Lestari, J. Wang, Curvature mode shape-based damage detection in composite laminated plates, Compos. Struct. 80 (3) (2007) 409–428.
[12] W. Xu, M. Cao, W. Ostachowicz, M. Radzienski, N. Xia, Two-dimensional curvature mode shape method based on wavelets and Teager energy for damage detection in plates, J. Sound Vib. 347 (2015) 266–278.
[13] W. Xu, M. Cao, X. Li, M. Radzienski, W. Ostachowicz, R. Bai, Delamination monitoring in CFRP laminated plates under noisy conditions using complex-wavelet 2D curvature mode shapes, Smart Mater. Struct. 26 (2017) 104008.
[14] W. Xu, K. Ding, J. Liu, M. Cao, M. Radzieński, W. Ostachowicz, Non-uniform crack identification in plate-like structures using wavelet 2D modal curvature under noisy conditions, Mech. Syst. Signal Process. 126 (2019) 469–489.
[15] Z.B. Yang, M. Radzienski, P. Kudela, W. Ostachowicz, Two-dimensional modal curvature estimation via Fourier spectral method for damage detection, Compos. Struct. 148 (2016) 155–167.
[16] Z.B. Yang, M. Radzienski, P. Kudela, W. Ostachowicz, Two-dimensional Chebyshev pseudo spectral modal curvature and its application in damage detection for composite plates, Compos. Struct. 168 (2017) 372–383.
[17] S. Cao, H. Ouyang, L. Cheng, Baseline-free multidamage identification in plate-like structures by using multiscale approach and low-rank modelling, Struct. Contr. Health Monit. 26 (2019), e2293.
[18] S. Cao, H. Ouyang, L. Cheng, Baseline-free adaptive damage localization of plate-type structures by using robust PCA and Gaussian smoothing, Mech. Syst. Signal Process. 122 (2019) 232–246.
[19] Y.F. Xu, W.D. Zhu, Non-model-based damage identification of plates using measured mode shapes, Struct. Health Monit. 16 (2017) 3–23.
[20] Y.F. Xu, W.D. Zhu, S.A. Smith, Non-model-based damage identification of plates using principal, mean and Gaussian curvature mode shapes, J. Sound Vib. 400 (2017) 626–659.
[21] D.M. Chen, Y.F. Xu, W.D. Zhu, Experimental investigation of notch-type damage identification with a curvature-based method by using a continuously scanning laser Doppler vibrometer system, J. Nondestr. Eval. 36 (2017) 38.
[22] D.M. Chen, Y.F. Xu, W.D. Zhu, Identification of damage in plates using full-field measurement with a continuously scanning laser Doppler vibrometer system, J. Sound Vib. 422 (2018) 542–567.
[23] D.M. Chen, Y.F. Xu, W.D. Zhu, Non-model-based identification of delamination in laminated composite plates using a continuously scanning laser Doppler vibrometer system, J. Vib. Acoust. 140 (2018), 041001.
[24] H. Xu, L. Cheng, Z. Su, J.L. Guyader, Damage visualization based on local dynamic perturbation: theory and application to characterization of multi-damage in a plane structure, J. Sound Vib. 332 (2013) 3438–3462.
[25] H. Xu, L. Cheng, Z. Su, Suppressing influence of measurement noise on vibration-based damage detection involving higher-order derivatives, Adv. Struct. Eng. 16 (2013) 233–244.
[26] M.S. Cao, W. Ostachowicz, M. Radzienski, W. Xu, Multiscale shear-strain gradient for detecting delamination in composite laminates, Appl. Phys. Lett. 103 (2013) 101910.
[27] A.W. Leissa, M.S. Qatu, Vibration of Continuous Systems, McGraw Hill, 2011.
[28] S. Mallat, A Wavelet Tour of Signal Processing, Academic Press, 2008.
[29] I.T. Jolliffe, Principal Component Analysis, Springer, 2011.
[30] W. Xu, Z. Su, J. Liu, M. Cao, W. Ostachowicz, Singular energy component for identification of initial delamination in CFRP laminates through piezo-electric actuation and non-contact measurement, Smart Mater. Struct. 29 (4) (2020), 045001.

[31] W. Xu, H. Fang, M. Cao, L. Zhou, Q. Wang, W. Ostachowicz, A noise-robust damage indicator for characterizing singularity of mode shapes for incipient delamination identification in CFRP laminates, Mech. Syst. Signal Process. 121 (2019) 183–200.
[32] W. Xu, M. Radzienski, W. Ostachowicz, M.S. Cao, Damage detection in plates using two-dimensional directional Gaussian wavelets and laser scanned operating deflection shapes, Struct. Health Monit. 12 (2013) 457–468.
[33] W. Xu, W.D. Zhu, S.A. Smith, M.S. Cao, Structural damage detection using slopes of longitudinal vibration shapes, J. Vib. Acoust. 138 (3) (2016), 034501.
[34] B. Park, H. Sohn, P. Malinowski, W. Ostachowicz, Delamination localization in wind turbine blades based on adaptive time-of-flight analysis of noncontact laser ultrasonic signals, Nondestr. Test. Eval. 32 (2017) 1–20.